



University of HUDDERSFIELD

University of Huddersfield Repository

Brethee, Khaldoon F., Gao, Jingwei, Ball, Andrew and Gu, Fengshou

Analysis of Frictional Effects on the Dynamic Response of Gear Systems and the Implications for Diagnostics

Original Citation

Brethee, Khaldoon F., Gao, Jingwei, Ball, Andrew and Gu, Fengshou (2015) Analysis of Frictional Effects on the Dynamic Response of Gear Systems and the Implications for Diagnostics. In: Proceedings of the 21st International Conference on Automation and Computing (ICAC). IEEE. ISBN 978-0-9926801-0-7

This version is available at <http://eprints.hud.ac.uk/id/eprint/26005/>

The University Repository is a digital collection of the research output of the University, available on Open Access. Copyright and Moral Rights for the items on this site are retained by the individual author and/or other copyright owners. Users may access full items free of charge; copies of full text items generally can be reproduced, displayed or performed and given to third parties in any format or medium for personal research or study, educational or not-for-profit purposes without prior permission or charge, provided:

- The authors, title and full bibliographic details is credited in any copy;
- A hyperlink and/or URL is included for the original metadata page; and
- The content is not changed in any way.

For more information, including our policy and submission procedure, please contact the Repository Team at: E.mailbox@hud.ac.uk.

<http://eprints.hud.ac.uk/>

Analysis of Frictional Effects on the Dynamic Response of Gear Systems and the Implications for Diagnostics

Khaldoon F. Brethee¹, Jingwei Gao², Fengshou Gu¹, Andrew D. Ball¹

¹Centre for Efficiency and Performance Engineering, University of Huddersfield, Huddersfield, HD1 3DH.

²Basic Education College, National University of Defense Technology, Changsha, China
khaldoon.brethee@hud.ac.uk

Abstract—To develop accurate diagnostic techniques, this study examines gear dynamic responses based on a model including the frictional effect of tooth mesh process. An 8-DOF (degree-of-freedom) model is developed to include the effect of not only gear dynamics but also supporting bearings, a driving motor and a loading system. Moreover, it takes into account the nonlinearity of both the time varying stiffness and the time-varying forces due to the friction effect. The latter causes additional vibration responses in the direction of the off-line-of-action (OLOA). To show the quantitative effect of the friction, vibration responses are simulated under different friction coefficients. It shows that an increase in friction coefficient value causes a nearly linear increase in the vibration features. However, features from torsional responses and the principal responses in the line-of-action (LOA) show less changes in the vibration level, whereas the most significant increasing is in the OLOA direction. In addition, the second and third harmonics of the meshing frequency are more influenced than the first harmonic component for all motions. These vibration responses are more sensitive for indicating lubrication changes and enhancing conventional diagnostic features.

Keywords—diagnosis; sliding velocity; friction coefficient; vibration response; simulation;

I. INTRODUCTION

In order to achieve accurate diagnostics, a significant number of studies have been carried out on the modelling and simulation of gear dynamics. They have resulted in a wide variety of dynamic models available to predict the response of gear vibration in order to improve the current techniques of diagnosis and monitoring [1]. Simulation can be very valuable for gaining a better understanding of complex interaction between transmission components in a dynamic environment and hence improving machine diagnostics and prognostics. It helps to develop effective signal processing methods for characterizing complicated weak fault signatures contaminated by different noises [2]. Therefore, different dynamic models for various gearbox systems were presented in [3-8]. In which both torsional and translational vibration responses of gears were studied as a tool for aiding gearbox diagnostic inferences. Moreover, vibration relating to gear spalling

or tooth breakage [5, 9-11], tooth crack [12-15], tooth surface pitting and wear [16-19] have been used to study these faults in terms of gear fault monitoring and diagnostics. In general, these models included both translation and rotational motions to show the fault effects on the dynamic characteristics. However, most of presented models ignored the friction effect or did not consider the friction between gear tooth contacts effectively, which may give less accuracy of diagnostic results.

In the meantime, sliding friction between the tooth surfaces has been reported to be one of the main sources of power loss in geared transmissions as well as an effective source of undesired vibration and noise [20-22]. A six-degree-of-freedom dynamic model of a spur gear pair influenced by friction was proposed in [23, 24], which was used to examine gear design modifications on the gear dynamic responses. Cheng-zhong et al [25] and Howard et al [26] detailed gear dynamic model to study the friction effect on some vibration characteristics of the gears, but they did not signify the friction effects precisely.

This study develops a comprehensive model coupling with tooth friction and necessary transmission components. Then a series of simulation studies are carried out to investigate the characteristics of vibration features when a gearbox is influenced by different frictional cases. In particular, the mesh components will be examined in order to define effective and accurate vibration features for monitoring tooth surface defects and lubrication conditions.

II. MESHING MODEL

A. Gear Tooth Meshing Process

The relative contact motions between two compressed elastic bodies (gear teeth) are the origin of internal excitations of vibration in gearing. They result in contacting forces that act on both bodies with the same intensity but in opposite directions. Especially, these forces cause impacts at transitions of gear tooth meshing events within a mesh cycle. As shown in Fig. 1, the transition can be determined from the un-deformed gear

pair geometry. The line AB represents the line of action (LOA) between the tangential points to the base circle of the gears. There are four regions along AB due to the change of tooth pairs in contact. The actual zone of the line of action (LOA = CF) is represented as the line between the intersection of the addendum circle of pinion and gear with the line AB (points C and F). D and E are two points on the line AB such that $CE=DF=p_b$, where p_b is the base pitch of the gear tooth curve. Sections DP and PE are the single-tooth contact regions while sections CD and EF are the double-tooth contact regions. The main geometric relations of these regions used in this model are given by:

$$AB = (r_{bp} + r_{bg}) \tan \alpha = (r_p + r_g) \sin \alpha \quad (1)$$

$$LOA = CF = \sqrt{r_{ap}^2 - r_{bp}^2} + \sqrt{r_{ag}^2 - r_{bg}^2} - (r_p + r_g) \sin \alpha \quad (2)$$

$$AC = (r_p + r_g) \sin \alpha - \sqrt{r_{ag}^2 - r_{bg}^2} \quad (3)$$

$$AF = \sqrt{r_{ap}^2 - r_{bp}^2} \quad (4)$$

$$FB = (r_p + r_g) \sin \alpha - \sqrt{r_{ap}^2 - r_{bp}^2} \quad (5)$$

$$CE = DF = p_b = \frac{2\pi r_{bp}}{Z_1} = \frac{2\pi r_{bg}}{Z_2} \quad (6)$$

$$P_{angle} = \frac{2\pi}{Z_1} \quad (7)$$

$$\varepsilon_{ratio} = \frac{CF}{p_b} \quad (8)$$

$$\psi_{sp} = \tan^{-1} \left(\frac{AC}{r_{bp}} \right) \quad (9)$$

$$\psi_{ep} = \tan^{-1} \left(\frac{AF}{r_{bp}} \right) - \psi_{sp} \quad (10)$$

where α is the pressure angle and the ratio of the length of contact path to the base pitch is recognized as the contact ratio ε_{ratio} of a gear pair. The start angle of mesh cycle is named by ψ_{sp} while the end angle of LOA is ψ_{ep} as illustrated in Fig. 1. In addition, the time-varying moment arms $\rho_p(t)$ and $\rho_g(t)$ for the i^{th} meshing pair can be found by:

$$\rho_p(t) = AC + \text{mod}(r_{bp} \omega_p, p_b) \quad (11)$$

$$\rho_g(t) = FB + \text{mod}(r_{bg} \omega_g, p_b) \quad (12)$$

where the function $\text{mod}(x, y) = x - y \cdot \text{floor}(x/y)$ is the modulus function, if $y \neq 0$, ω_p and ω_g are the nominal speeds in (rad/s), and AC and FB are the geometric length constants. The sliding friction forces on each contact pair are denoting by F_{p1} , F_{g1} , F_{p0} and F_{g0} respectively.

These forces affect gear rotations by frictional torques about the gear centres and excite the off-line-of-action gear translations significantly as it will be explained later in form of $F_{fi}(t)$.

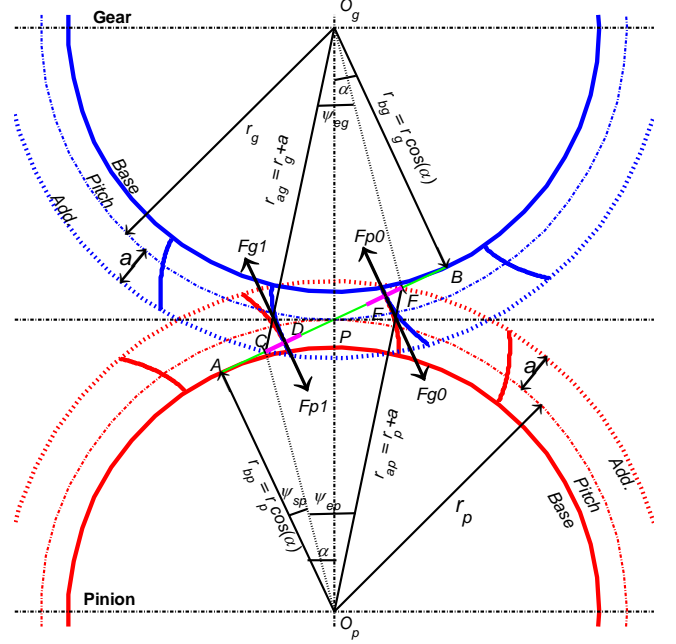


Figure 1 Meshing process of spur gear pairs

B. Varying Meshing Stiffness

The major variations in gear stiffness are caused by changes in meshing pair number. Spur gears have single-tooth and double tooth meshing appearing alternately during the process of mesh [27]. For normal spur gears with a contact ratio of more than one, the meshing pair numbers usually in the range between 1.0 and 2.0 [25, 28]. In existing literature, the tooth meshing stiffness is simplified as a rectangular wave [29] based on the equal load sharing formulation, which proposed by Vaishya and Singh in [22, 30, 31]. The existing model considered the sudden changing in the meshing stiffness value by a periodic square wave function at every stage. It makes the single-tooth meshing and the double tooth meshing appears alternately and changes suddenly during the mesh transitions. Figure 2(a) explains the various positions of gear tooth meshing events for identical spur gears within a pinion pitch duration angle P_{angle} as in (7). The dynamic model considers the pair of spur gears as two rigid disks coupled along the line of action through a time varying mesh stiffness $k(t)$ and damping $c(t)$ [28]. The mesh contact cycle starts from the angle ψ_{sp} at point C, denoting as the starting point of contact, where the addendum circle diameter of the gear intersects the active line of action (LOA). The mesh period of double pair tooth contact (M_{double}) begins when pair1 contact at point C whereas pair 0 is already in contact at point E, which is denoting as the ending point of single tooth contact. As the gears rotate, within the angle ψ_{ep} , the points of contact move along the line of action CF. When the pair 1 reaches the point D (the starting point of single tooth

contact), pair 0 disengages at point F (the finishing point of the mesh cycle) and leaves only the pair 1 in the single contact zone (M_{single}). In addition, while pair 1 reaches to point E, the next tooth pair engages at point C which starts another mesh cycle. Finally, when pair 1 rotates to point F, one meshing cycle is completed. Therefore, the meshing process leads to mesh stiffness that varying with time as illustrated in Fig. 2(b).

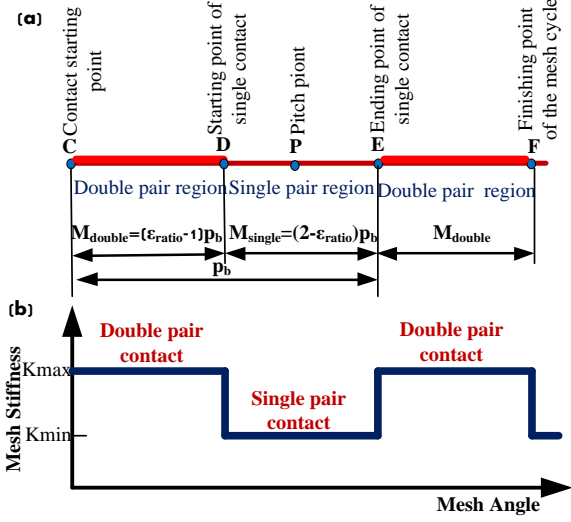


Figure 2 Mesh stiffness regions of meshing gear pair in one period

C. Varying Friction Effects between Tooth Surfaces

Friction forces and the nonlinearity excitation between tooth contact surfaces are the main sources of vibration [23]. Due to the velocity reversion at pitch point, friction can be associated with a large oscillatory component due to high forces in the sliding direction. The sliding velocity for each tooth pair in contact can be derived from meshing kinematics and oscillating torsional motion of the gear and pinion. This dependency upon the implicit non-linearity of vibrating velocity in the gear dynamic system [22]. The normal contact force and the friction force between pair of gears is calculated by Howard et al. [32], which is modelled as the combination of linear elastic and damping forces as shown in Fig. 3(a),

$$N_i = C(t)(r_{p1}\dot{\theta}_1 - r_{g1}\dot{\theta}_2 - \dot{y}_{p1} + \dot{y}_{g1}) + K_{mi}(t)(r_{p1}\theta_1 - r_{g1}\theta_2 - y_{p1} + y_{g1}) \quad (13)$$

where $i=0, 1$ denoting meshing tooth pair. The surface friction generated between the meshing tooth surfaces are:

$$F_{fi}(t) = \mu N_i \quad (14)$$

The dynamic friction formulation is modelled as a time-varying parameter; see Fig. 3(b). The friction coefficient (μ_0) formula of tooth surface is stated as constant; however it changes its sign with the direction of relative sliding velocity, i.e.

$$\mu = \mu_0 \operatorname{sgn}(V_s) = \begin{cases} \mu_0 & , V_s > 0 \\ -\mu_0 & , V_s < 0 \end{cases} \quad (15)$$

where, V_s refers to the sliding velocity at the contact point of interest. The sliding velocity is considered as the difference between surface velocities at each contact point. For i^{th} gear pair, its sliding velocity is:

$$V_{si} = \rho_{pi}(t)\omega_p - \rho_{gi}(t)\omega_g \quad (16)$$

For individual gear and pinion, $\rho(t)$ and ω are the radius of curvature of the corresponding contact point and the angular velocity of precise gear respectively. Hence, the friction moment of the pinion and gear is produced by the tooth friction forces $F_{fi}(t)$ and friction arms $\rho_i(t)$:

$$\left. \begin{aligned} T_{fp}(t) &= \rho_{pi}(t) F_{fi}(t) \\ T_{fg}(t) &= \rho_{gi}(t) F_{fi}(t) \end{aligned} \right\} \quad (17)$$

The direction of friction torque is dependent on the instantaneous sliding velocity and the contact point location as illustrated in Fig. 3(c).

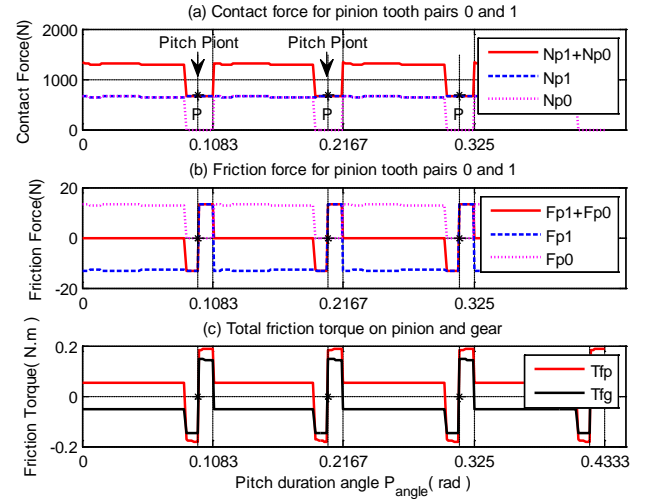


Figure 3 Variation of normal contact forces, friction forces and frictional torque with the pitch period

D. Friction Coefficient

Many parameters affect friction coefficient μ_0 because of the complex lubricating problem in gearing. Different empirical formulae were proposed to estimate the friction coefficient [33]. However, these empirical formulae for μ_0 , valid within certain ranges of key system parameters. They are not general and often represent certain lubricants, operating temperatures, speed and load ranges, and surface roughness conditions of roller specimens that might differ from those of the actual gear pair of interest [33]. In general, the theoretical friction coefficient is derived from elasto-hydrodynamic lubrication and tribology theory, however several experimental works show that, a constant friction coefficient is acceptable for dynamic analysis as indicated in [34-36]. Benedict and Kelley's empirical equation shows that, the coefficient of friction varies between 0.03 to 0.1 [37], furthermore the value of 0.1 or even values as high as 0.2 are commonly used in several gear dynamic models as explained in [36]. To get meaningful values of μ_0 , the variation from 0.0 to 0.2 have been used in this study to simulate the Coulomb

friction effect. The friction coefficient function is determined by the direction of the sliding velocity as represented in (15). The variation in sliding velocity (16) can be shown in Fig. 4(a), which gives a variant square wave shape during the mesh period. For example, a constant friction coefficient ($\mu_0=0.02$) is represented in Fig. 4(b). It can be seen that, a significant changes in μ_0 give an effective simulation to the friction coefficient during the meshing process.

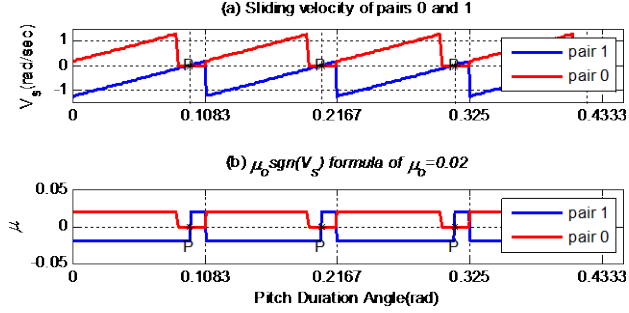


Figure 4 Sliding velocity and friction coefficient function of pair0 and pair1 during the mesh period

III. DYNAMIC MODEL AND SOLUTION METHOD

A. Gear Dynamic Model

To investigate friction influences, the model considered in this research is based on the one developed and subsequently modified by Kahraman [23] and Singh [24]. However, to represent gear transmission more accurately, the model also takes into account effects of speed-torque characteristics of motor driving systems. As shown in Fig. 5, the model is an 8-degree-of-freedom nonlinear model. The pinion and gear, denoted with subscripts 1 and 2 respectively have translational motions and rotational motions. As shown by the geometric specification in Table 1, the gear system is a speed increaser which is the same configuration as wind turbine applications. The pinion and gear are coupled by a spring having time varying mesh stiffness $K_m(t)$ and a varying mesh damping $C_m(t)$. The model includes four inertias, namely load, motor, pinion and gear. The torsional compliances of shafts and the transverse compliances of bearings combined with those of shafts are included in the model. The resilient elements of supports are described by stiffness and damping coefficients K_{x1} , K_{x2} , C_{x1} and C_{x2} for the pinion and gear respectively in the OLOA direction, besides K_{y1} , K_{y2} , C_{y1} and C_{y2} in the LOA direction. The shafts between the input motor, output loading motor and the gears are represented by torsional stiffness and torsional damping components k_1 , k_2 , c_1 and c_2 . Moreover, the model takes into account the influence of torque T_m and T_L as the driving torque and load torque respectively. The transverse vibrations of the gears are considered along LOA and off-line of action (OLOA).

The equation of motions are arranged into the state space formulation base on vibration analysis and then with MATLAB operation supported by ODE solver. The governing equations of motion for the model depicted in

Fig. 5 are written based on the following key assumptions:

- Pinion and gear are modelled as rigid disks;
- Applying input torque and applied load to the system;
- Shaft mass and inertia are lumped at the gears;
- Coulomb friction is assumed with a constant coefficient of friction μ_0 ;
- Manufacturing and assembly errors are ignored;
- Static transmission error effects are neglected;
- Backlash is not considered in this model.

• Table 1 Geometric property of the meshing gears

Geometric Properties	Pinion	Gear
Number of teeth	$Z_p=58$	$Z_g=47$
Pitch radius (mm)	$r_p=40.08$	$r_g=32.48$
Mass (kg)	$m_p=0.86$	$m_g=0.68$
Rotation speed (rpm)	1485	1832.6
Pressure angle ($^\circ$)	$\phi = 20$	
Module (mm)	$m=1.38$	
Addendum (mm)	$a=1.4$	
Contact ratio	$\epsilon_{ratio} = 1.7822$	
Motor torque (Nm)	$M_0=36$	
Applied torque (Nm)	$T_L= 29.2$	

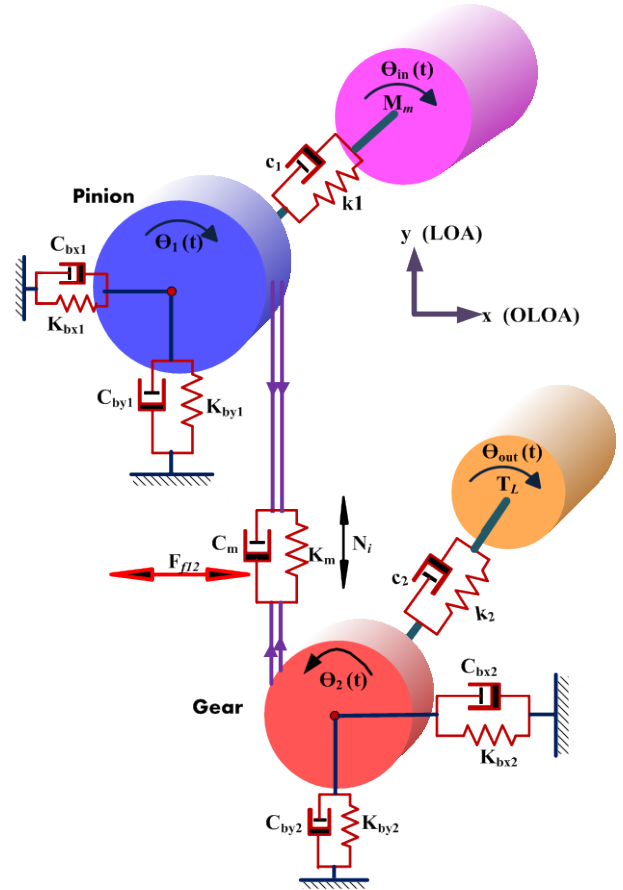


Figure 5 Schematic diagram of gear dynamic model with friction

According to the Newtonian law the equations of the motion are for the motor rotor, pinion rotation, gear rotation, Y-direction of pinion and gear translations, X direction of pinion and gear translations and load rotor respectively:

$$I_m \ddot{\theta}_{in} + c_1 (\dot{\theta}_{in} - \dot{\theta}_1) + k_1 (\theta_{in} - \theta_1) = M_m \quad (18)$$

$$I_p \ddot{\theta}_1 - c_1 (\dot{\theta}_{in} - \dot{\theta}_1) - k_1 (\theta_{in} - \theta_1) + r_p C_m (r_p \dot{\theta}_1 - r_g \dot{\theta}_2 + \dot{y}_p - \dot{y}_g) + r_p K_m (r_p \theta_1 - r_g \theta_2 + y_p - y_g) + F_{f12} \rho_p(t) = 0 \quad (19)$$

$$I_g \ddot{\theta}_2 + c_2 (\dot{\theta}_2 - \dot{\theta}_{out}) + k_1 (\theta_2 - \theta_{out}) - r_g C_m (r_p \dot{\theta}_1 - r_g \dot{\theta}_2 + \dot{y}_p - \dot{y}_g) - r_g K_m (r_p \theta_1 - r_g \theta_2 + y_p - y_g) - F_{f12} \rho_g(t) = 0 \quad (20)$$

$$I_L \ddot{\theta}_{out} - c_2 (\dot{\theta}_2 - \dot{\theta}_{out}) - k_1 (\theta_2 - \theta_{out}) = -T_L \quad (21)$$

$$m_p \ddot{y}_p + C_m (r_p \dot{\theta}_1 - r_g \dot{\theta}_2 + \dot{y}_p - \dot{y}_g) + K_m (r_p \theta_1 - r_g \theta_2 + y_p - y_g) + C_{by1} \dot{y}_p + K_{by1} y_p = 0 \quad (22)$$

$$m_g \ddot{y}_g - C_m (r_p \dot{\theta}_1 - r_g \dot{\theta}_2 + \dot{y}_p - \dot{y}_g) - K_m (r_p \theta_1 - r_g \theta_2 + y_p - y_g) + C_{by2} \dot{y}_g + K_{by2} y_g = 0 \quad (23)$$

$$m_p \ddot{x}_p + C_{bx1} \dot{x}_p + K_{bx1} x_p - F_{f12} = 0 \quad (24)$$

$$m_g \ddot{x}_g + C_{bx2} \dot{x}_g + K_{bx2} x_g + F_{f12} = 0 \quad (25)$$

$$M_m = M_m + 10(\omega_p - \dot{\theta}_1) \quad (26)$$

Equation (26) is used to adjust the motor input torque to maintain its speed as constant as possible. Especially, additional static torque is needed in order to balance the torque due to friction effects. This torque adaptation is to simulate the speed-torque characteristics for a common induction motor used widely. So that, a slight changes in the motor parameters will be predicted as it will explain later.

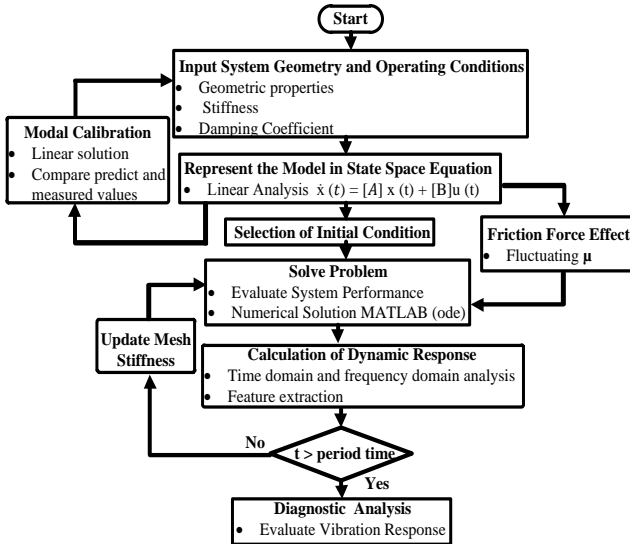


Figure 6 Simulation procedure used in this study

B. Solution Procedure

A numerical simulation study was performed to obtain the solution of the nonlinear equations. However, to ensure the correctness of parameters used and model structures, linear solutions was obtained when an average meshing stiffness value is used in the model without fiction influences, which allows the adjustment of the

model parameters so that major resonances agree with real system as close as possible. Subsequently, the non-linear effects of varying friction and mesh stiffness have been applied to the model and numerical integration method is used to solve the model. The difference of the gear vibration responses are examined between different friction coefficient values. More details of the simulation procedure used in this study are summarized in a flowchart shown in Fig. 6.

IV. MODAL CALIBRATION

A. Linear Solution

A simplified linear version of this model is developed by using the average mesh stiffness value in (19)-(23). It allows modal parameters including resonance frequencies and damping ratios to be found conveniently using the standard eigen method. By considering linear factors of the system, the vibration differential equation is expressed as:

$$[M]\{\ddot{q}\} + [C]\{\dot{q}\} + [K]\{q\} = f(t) \quad (27)$$

$$\{\dot{V}\} = [A]\{q\} \quad (28)$$

where, $[M]$ is mass matrix, $[C]$ is damping matrix, $[K]$ is stiffness matrix and q is vibration response vector consisting of displacements and velocity of the system. Using standard method for linear system analysis, the frequency response can be obtained conveniently under different parameters settings. Figure 7 shows the system responses with refined parameters. It can be seen that the 1st mode is at 128Hz which is 4 times away from the shaft frequency at about 25Hz. The third and fourth modes are close to the 2nd harmonic of $2 \times f_m = 2 \times f_r Z = 2 \times 1435.5 Hz$.

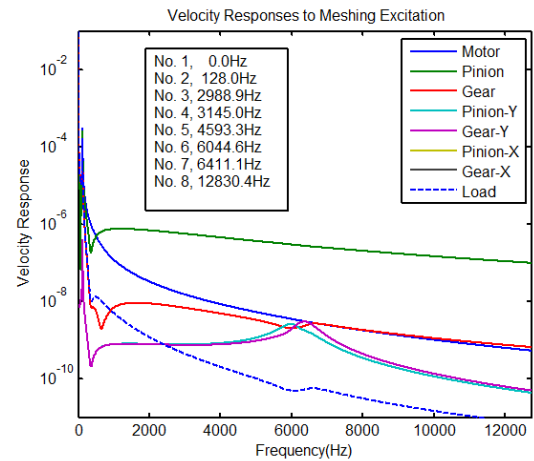


Figure 7 Frequency responses of gear system excited with impulsive inputs at the pinion and gear

To maintain the solution stability in the case of solving the nonlinear equations, these modes are applied with high damping ratios so that the frequency responses around these frequency ranges are relatively flat. Also note that there is no response in X-directions as there is no friction effect included in the linear mode. Moreover

the frequency responses are similar to that of measurements from the gearbox installed in the lab. It shows that the key parameters such as tooth stiffness values and damping ratios are used appropriately and numerical solutions can be proceeded to obtain the nonlinear responses.

B. Nonlinear Solution

The time domain behavior of the nonlinear system is obtained by integrating the set of governing differential equations numerically using an ode15s Runge–Kutta algorithm with a fixed time step size. This is suitable for solving differential algebraic stiff problems with high fluctuations and large noises in the solution. An appropriate set of initial conditions was applied to integrate the problem. The operating conditions of the system observed convergent responses corresponding to constant speed of interest. Figure 8 presents acceleration responses in the time domain and frequency domain for a case with friction included. In the time domain, all the responses including pinion and gears in rotations (θ_1 , θ_2), translations in the LOA (y_p , y_g) and OLOA (x_p , x_g) directions exhibit periodic profiles following stiffness changes, which is confirmed in the frequency domain in which the spectral peaks are observed at the gear mesh frequency $f_m = f_r Z = 1435.5\text{Hz}$ and its higher order harmonics. This spectral pattern is of typical for gear vibrations. However, because of the effect of resonances, the amplitudes at the higher order harmonics are higher than the fundamental one. For the same reasons, the rotational response of the pinion is higher than that of the gear, which is also seen in the frequency response characteristics.

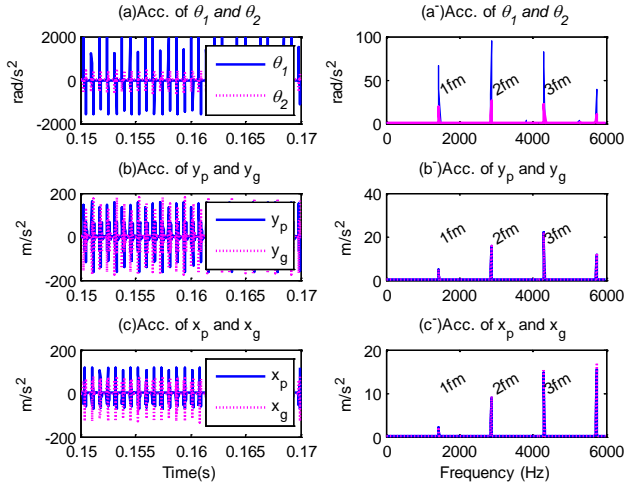


Figure 8 Vibration responses in the time domain and frequency domain

V. SIMULATION RESULTS AND DISCUSSION

A. Speed and Transmission Power

Having confirmed that the general solution of the system is close to reality, simulation studies were performed under a successive increment of friction coefficients μ_o from 0 and 0.2 which is the range explored in previous studies. The operating conditions

were kept exactly the same for different values of coefficients. The load torque is $T_L = 29.2\text{Nm}$, which corresponds an input torque 36 Nm at the speed of 1485 rpm.

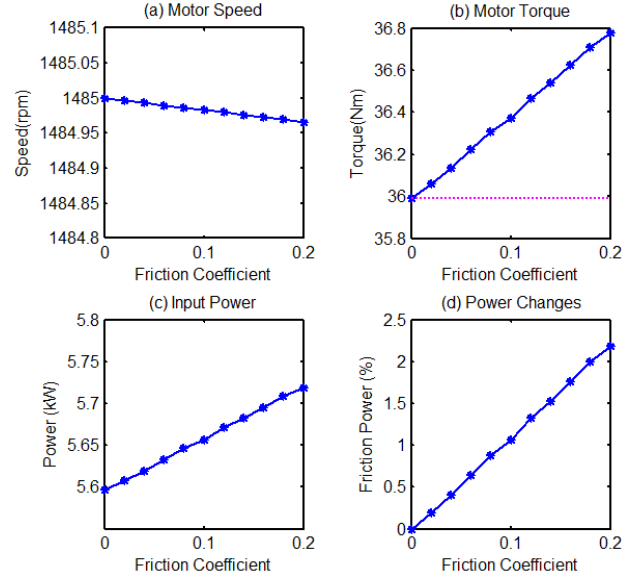


Figure 9 Effect of friction on motor operating parameters

Figure 9 shows the change of operating parameters with friction coefficient. It can be seen that there is a slight drop in the speed but a significant increase in the input torque. It means that with more friction effect, more input power is required to maintain the speed as close as to the setting point. However, because of the torque adaptation of (26) used, the speed has such a slight drop. Moreover, it is observed that there is a nearly linear increase in the motor power and the maximum change is 2.18%. It shows that it is clear that power measurement can be used for indicating lubrication degradation. These changes in operating conditions show that the model prediction is consistent with real operations and hence the vibration responses can be examined realistically.

B. Vibration Responses

Commonly, accelerations are measured for monitoring machine vibration characteristics. So the numerical solutions are converted into accelerations by differentiating the velocity responses. In addition to calculating the root mean squared (RMS) values for examining changes in overall vibration levels, spectral amplitudes at meshing frequencies are also extracted from the spectra of the acceleration responses in order to obtain a quantities assessment of frictional effect on default diagnostic features. As shown in Fig 10, RMS values for nearly all vibration signals show a monotonous increase, which is consistent with that of previous studies for noise reduction. However, because of the effect of nonlinearity, the response of the gear rotation exhibit quadratic nonlinear increase. In general, the vibration response increases with friction. Therefore, higher vibration level may indicate that the lubrication condition is poorer.

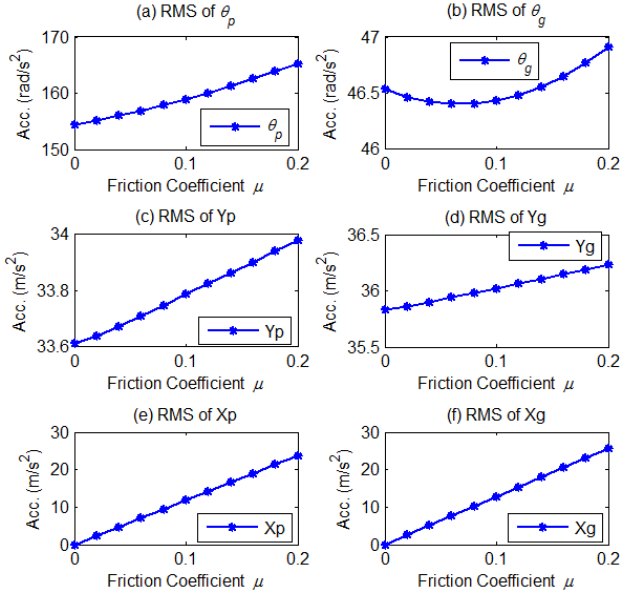


Figure 10 RMS of acceleration signals in rotation and translation transverse for pinion and gear

C. Vibration at Meshing Frequency

For more detailed and accurate friction diagnosis, the change of spectral amplitudes is usually indicating the gearbox conditions. Figure 11 presents the first three harmonic components of rotational responses for the meshing frequency. It can be seen that they behave diversely. The first and the third harmonics on the pinion show a nearly linear increase trend with friction, which can be based on the friction effect indicator. However, due to the nonlinear responses, the three components of the gear show inverse change and may not be so direct to be taken as good indicator for frictional influences.

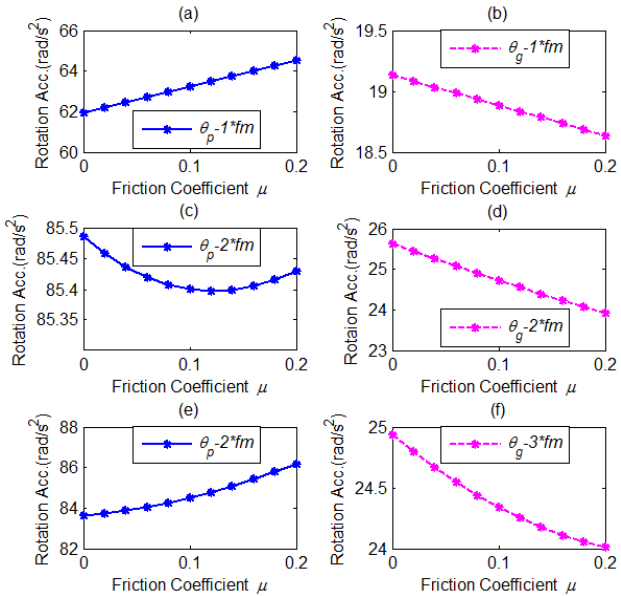


Figure 11 Rotation responses at mesh frequency with friction

In the same way the the nonlinear response also cause the second and the third harmonic components of the translational responses in Y-direction to decrease with increasing in friction, as showing in Fig. 12. However,

the first harmonic increases with the friction coefficient and hence can be based on to indicate the change of friction due to lubricant degradation.

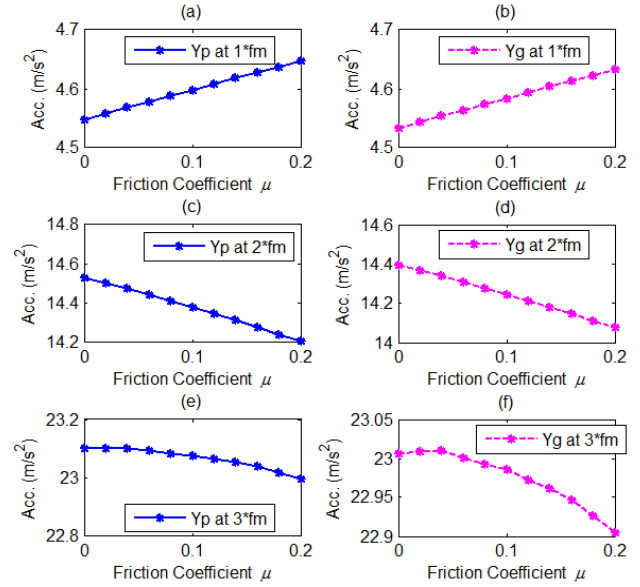


Figure 12 Spectral peaks of translation responses in Y-direction (LOA)

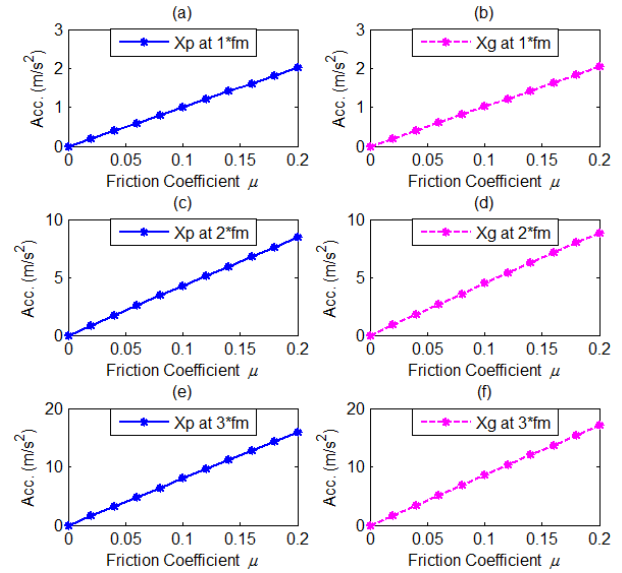


Figure 13 Spectral peaks of translation responses in X-direction (OLOA)

For the translation responses in X-direction, all harmonic components exhibit good increase trend that is proportional to the friction coefficient. Therefore, any of them can be used for lubrication condition monitoring. Moreover, the amplitude of increase is more significant, compared with the changes in the Y-direction. Therefore, the combination of the responses in two directions could result in an overall increase trend, which represents the real measurement values perceived by a sensor on the housing of a gearbox. Figure 14 is the combined responses obtained by $a_{xy} = \sqrt{a_x^2 + a_y^2}$ provided that the frequency response of housing is in linear range. As shown in the figure, the entire three component exhibit as

a monotonous increase with friction and it can be effective indicators for the friction. Moreover, as the change is tiny for the small friction coefficients, it means that vibration responses measured on the housing are relatively stable for good lubrication conditions. In other words, diagnostic features for other fault such as tooth breakages are also stable for obtaining a reliable severity diagnostic result. In the meanwhile, the diagnostic features will be further enlarged by poor lubrications, which is helpful to detect incipient tooth problems.

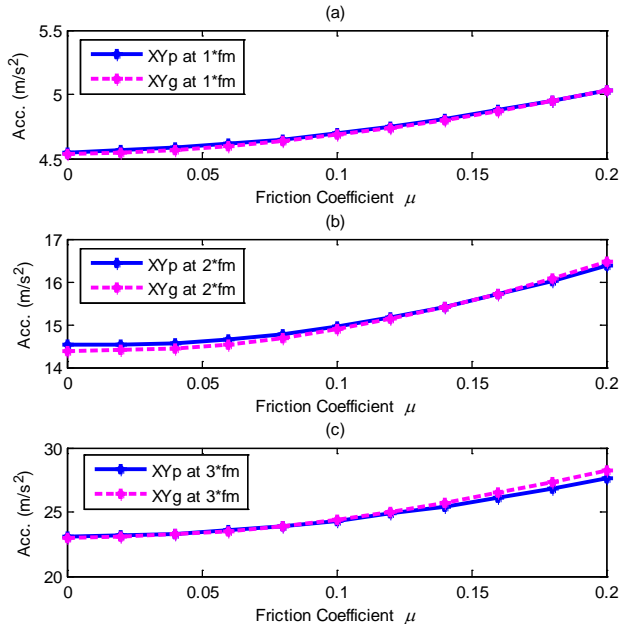


Figure 14 Spectral peaks of combined translation responses

In addition, the combined responses also show that the difference of the responses between the pinion and gear is very close, which means that the measurement at a position near either to the pinion or the gear will produce the same results for monitoring.

CONCLUSION

The dynamic model coupling with tooth friction produces consistent vibration responses to the change in friction due to lubrication degradation. It shows that there is an increase up to 2.18% in power consumption due to friction coefficient changes. However, the maximum increase of vibration responses of spectral peaks can be more than 100%. These show that it is much significant to use vibration responses to monitor the change in friction behavior. In the meantime, the power consumption may need a more accurate measurement system to resolve the small changes.

Both rotational responses and translational responses of vibration can be good indicators for lubrication conditions but the translational one is more sensitive even though the rotational responses are generally more nonlinear.

REFERENCES

[1] Randall, R., *A new method of modeling gear faults*. Journal of Mechanical Design, 1982. **104**(2): p. 259-267.

[2] Jardine, A.K., D. Lin, and D. Banjevic, *A review on machinery diagnostics and prognostics implementing condition-based maintenance*. Mechanical systems and signal processing, 2006. **20**(7): p. 1483-1510.

[3] Begg, C.D., et al. *Dynamics modeling for mechanical fault diagnostics and prognostics*. in *Maintenance and Reliability Conf.* 1999.

[4] Bruns, C.J., *Dynamic gearbox simulation for fault diagnostics using a torque transducer*. 2011.

[5] Begg, C.D., C.S. Byington, and K.P. Maynard. *Dynamic simulation of mechanical fault transition*. in *Proceedings of the 54th Meeting of the Society for Machinery Failure Prevention Technology, Virginia Beach, VA*. 2000.

[6] Bartelmus, W., *Mathematical modelling and computer simulations as an aid to gearbox diagnostics*. Mechanical Systems and Signal Processing, 2001. **15**(5): p. 855-871.

[7] Van Khang, N., T.M. Cau, and N.P. Dien, *Modelling parametric vibration of gear-pair systems as a tool for aiding gear fault diagnosis*. technische mechanik, 2004. **24**: p. 3-4.

[8] Diagnostics, R. and I. Gilon, *Gear Diagnostics—Fault Type Characteristics*.

[9] Chaari, F., et al., *Effect of spalling or tooth breakage on gearmesh stiffness and dynamic response of a one-stage spur gear transmission*. European Journal of Mechanics-A/Solids, 2008. **27**(4): p. 691-705.

[10] Jia, S. and I. Howard, *Comparison of localised spalling and crack damage from dynamic modelling of spur gear vibrations*. Mechanical Systems and Signal Processing, 2006. **20**(2): p. 332-349.

[11] Lu, D., X. Gong, and W. Qiao. *Current-based diagnosis for gear tooth breaks in wind turbine gearboxes*. in *Energy Conversion Congress and Exposition (ECCE), 2012 IEEE*. 2012. IEEE.

[12] Tian, Z., M.J. Zuo, and S. Wu, *Crack propagation assessment for spur gears using model-based analysis and simulation*. Journal of Intelligent Manufacturing, 2012. **23**(2): p. 239-253.

[13] Wu, S., M.J. Zuo, and A. Parey, *Simulation of spur gear dynamics and estimation of fault growth*. Journal of Sound and Vibration, 2008. **317**(3): p. 608-624.

[14] Chen, Z. and Y. Shao, *Dynamic simulation of spur gear with tooth root crack propagating along tooth width and crack depth*. Engineering Failure Analysis, 2011. **18**(8): p. 2149-2164.

[15] Mohammed, O.D., M. Rantatalo, and J.-O. Aidanpää, *Dynamic modelling of a one-stage spur gear system and vibration-based tooth crack detection analysis*. Mechanical Systems and Signal Processing, 2015. **54**: p. 293-305.

- [16] Choy, F., et al., *Analysis of the Effects of Surface Pitting and Wear on the Vibrations of a Gear Transmission System*. 1994, DTIC Document.
- [17] Ding, H., *Dynamic Wear Models for Gear Systems*. 2007, The Ohio State University.
- [18] Ding, H., *A study of interactions between dynamic behavior of gear systems and surface wear*. 2007, The Ohio State University.
- [19] Flodin, A., *Wear of spur and helical gears*. Royal Institute of Technology, Stockholm, Doctoral Thesis, 2000.
- [20] Jiang, H., Y. Shao, and C.K. Mechefske, *Dynamic characteristics of helical gears under sliding friction with spalling defect*. *Engineering Failure Analysis*, 2014. **39**: p. 92-107.
- [21] Diab, Y., F. Ville, and P. Velex, *Investigations on power losses in high-speed gears*. *Proceedings of the Institution of Mechanical Engineers, Part J: Journal of Engineering Tribology*, 2006. **220**(3): p. 191-198.
- [22] Vaishya, M. and R. Singh, *Sliding friction-induced non-linearity and parametric effects in gear dynamics*. *Journal of Sound and Vibration*, 2001. **248**(4): p. 671-694.
- [23] Kahraman, A., J. Lim, and H. Ding. *A dynamic model of a spur gear pair with friction*. in *Proceedings of the 12th IFToMM World Congress*. 2007.
- [24] He, S., S. Cho, and R. Singh, *Prediction of dynamic friction forces in spur gears using alternate sliding friction formulations*. *Journal of Sound and Vibration*, 2008. **309**(3): p. 843-851.
- [25] Cheng-zhong, G. and C. Lie. *Effects of teeth surface friction on the vibration of gear transmission*. in *Mechanical and Electronics Engineering (ICMEE), 2010 2nd International Conference on*. 2010. IEEE.
- [26] Howard, I., S. Jia, and J. Wang, *The dynamic modelling of a spur gear in mesh including friction and a crack*. *Mechanical systems and signal processing*, 2001. **15**(5): p. 831-853.
- [27] Shing, T.-K., *Dynamics and control of geared servomechanisms with backlash and friction consideration*. 1994.
- [28] Kokare, D. and S. Patil, *Numerical Analysis of variation in mesh stiffness for Spur Gear Pair with Method of Phasing*. 2014.
- [29] Lin, J. and R.G. Parker, *Mesh stiffness variation instabilities in two-stage gear systems*. *Journal of vibration and acoustics*, 2002. **124**(1): p. 68-76.
- [30] Vaishya, M. and R. Singh, *Analysis of periodically varying gear mesh systems with Coulomb friction using Floquet theory*. *Journal of Sound and Vibration*, 2001. **243**(3): p. 525-545.
- [31] Vaishya, M. and R. Singh, *Strategies for modeling friction in gear dynamics*. *Journal of Mechanical Design*, 2003. **125**(2): p. 383-393.
- [32] Jia, S., I. Howard, and J. Wang, *The dynamic modeling of multiple pairs of spur gears in mesh, including friction and geometrical errors*. *International Journal of Rotating Machinery*, 2003. **9**(6): p. 437-442.
- [33] Xu, H., *Development of a generalized mechanical efficiency prediction methodology for gear pairs*. 2005, The Ohio State University.
- [34] Velex, P. and V. Cahouet, *Experimental and numerical investigations on the influence of tooth friction in spur and helical gear dynamics*. *Journal of Mechanical Design*, 2000. **122**(4): p. 515-522.
- [35] Rebbeschi, B., F.B. Oswald, and D.P. Townsend, *Measurement of Gear Tooth Dynamic Friction*. 1996, DTIC Document.
- [36] Liu, G., *Nonlinear dynamics of multi-mesh gear systems*. 2007, The Ohio State University.
- [37] He, S., R. Gunda, and R. Singh, *Effect of sliding friction on the dynamics of spur gear pair with realistic time-varying stiffness*. *Journal of Sound and Vibration*, 2007. **301**(3): p. 927-949.